Biophysical *Journal*
Article

Biophysical Society

Image-Based Measurement of H_2O_2 Reaction-Diffusion in Wounded Zebrafish Larvae

Mark Jelcic,[1,2] Balázs Enyedi,[4] João B. Xavier,[3,*] and Philipp Niethammer[1,*]
[1]Cell Biology Program, [2]Louis V. Gerstner, Jr. Graduate School of Biomedical Sciences, and [3]Computational and Systems Biology Program, Memorial Sloan Kettering Cancer Center, New York, New York; and [4]Department of Physiology, Faculty of Medicine, Semmelweis University, Budapest, Hungary

ABSTRACT Epithelial injury induces rapid recruitment of antimicrobial leukocytes to the wound site. In zebrafish larvae, activation of the epithelial NADPH oxidase Duox at the wound margin is required early during this response. Before injury, leukocytes are near the vascular region, that is, ~100–300 μm away from the injury site. How Duox establishes long-range signaling to leukocytes is unclear. We conceived that extracellular hydrogen peroxide (H_2O_2) generated by Duox diffuses through the tissue to directly regulate chemotactic signaling in these cells. But before it can oxidize cellular proteins, H_2O_2 must get past the antioxidant barriers that protect the cellular proteome. To test whether, or on which length scales this occurs during physiological wound signaling, we developed a computational method based on reaction-diffusion principles that infers H_2O_2 degradation rates from intravital H_2O_2-biosensor imaging data. Our results indicate that at high tissue H_2O_2 levels the peroxiredoxin-thioredoxin antioxidant chain becomes overwhelmed, and H_2O_2 degradation stalls or ceases. Although the wound H_2O_2 gradient reaches deep into the tissue, it likely overcomes antioxidant barriers only within ~30 μm of the wound margin. Thus, Duox-mediated long-range signaling may require other spatial relay mechanisms besides extracellular H_2O_2 diffusion.

INTRODUCTION

H_2O_2 is a diffusible and relatively stable reactive oxygen species that may act as an early, paracrine wound signal during tissue inflammation and regeneration (1–8). Tail fin tip amputation of larval zebrafish generates a tissue-scale gradient of H_2O_2 through Ca^{2+}-dependent activation of the epithelial NADPH oxidase Duox. This gradient extends >100 μm from the wound site into the tissue. Duox activity is required for rapid leukocyte recruitment to the wound (7). The mechanism of H_2O_2-induced leukocyte recruitment is phylogenetically conserved, but still incompletely understood.

Mechanisms of H_2O_2-dependent redox signaling often involve reversible thiol oxidation of amino acid residues (thiol switches) in transcription factors, kinases, phosphatases, and other regulatory proteins (9). In zebrafish and *Drosophila*, H_2O_2-mediated wound attraction of leukocytes requires oxidation of a redox-sensitive cysteine within the tyrosine kinase Lyn in leukocytes (10,11). Redox-sensitive cysteines may exhibit evolutionary conservation and functional relevance, although not all conserved and functionally relevant cysteines are necessarily redox-regulated. Importantly, the measured H_2O_2-reactivities of redox-sensitive thiols within nonantioxidant proteins are typically several orders of magnitude below those of professional antioxidants such as peroxiredoxin, which in some cells constitutes up to 1% of soluble protein (12,13). Hence, nonantioxidant, redox signaling proteins must compete with highly abundant antioxidants for H_2O_2. Few studies address how H_2O_2 can target regulatory thiol switches within this ocean of highly reactive H_2O_2-scavengers.

To explain this foundational riddle, it has been hypothesized that cellular antioxidant barriers must be breached by preceding pulses of H_2O_2 before H_2O_2 can signal to less reactive nonantioxidant proteins (14). Once antioxidant floodgates become leaky, cellular H_2O_2 degradation stalls or ceases. Whether, where, and when this occurs during wound redox signaling in tissues is, however, unclear. To test for floodgate breakage in vivo, we developed a computational method that directly computes H_2O_2 degradation rates from large time-lapse datasets of H_2O_2 biosensor imaging. Our data suggest that the wound-induced H_2O_2 gradient penetrates antioxidant floodgates close to the wound margin, but is less likely in distant leukocytes.

Submitted December 19, 2016, and accepted for publication March 27, 2017.

*Correspondence: xavierj@mskcc.org or niethamp@mskcc.org

Mark Jelcic and Balázs Enyedi contributed equally to this work.

Editor: Fazoil Ataullakhanov.
http://dx.doi.org/10.1016/j.bpj.2017.03.021

MATERIALS AND METHODS

Zebrafish procedures

Casper background Tg(actb2:HyPer) transgenic zebrafish (15) were maintained as described in Nüsslein-Volhard and Dahm (16) with the approval of the Institutional Animal Care and Use Committee (Memorial Sloan Kettering Cancer Center, New York, NY). Zebrafish larvae were raised in E3 medium (5 mM NaCl, 0.17 mM KCl, 0.33 mM $CaCl_2$, 0.33 mM $MgSO_4$). For wounding assays, 3.5–4-day postfertilization larvae were anesthetized using 0.2 mg/mL tricaine (Sigma-Aldrich, St. Louis, MO) in E3 for at least 20 min before wounding and during imaging.

Wide-field fluorescence microscopy of H_2O_2 gradients

Tg(actb2:HyPer) larvae were used to image the penetration of exogenous H_2O_2, and the generation of wound-induced, endogenous H_2O_2 gradients. Anesthetized larvae were subjected to tail fin tip amputation in isotonic E3 medium (iso-E3: E3 fish medium supplemented with 140 mM NaCl) using a needle knife (Fine Science Tools, Foster City, CA), and were embedded in a small volume of 1% isotonic, low-melting agarose (~50–70 μL) in a glass-bottom dish (MatTek, Ashland, MA) 1 h later. The waiting period was required for the endogenous, wound-induced H_2O_2 gradient to diminish, enabling the consecutive measurement of exogenous H_2O_2 gradients only. In experiments with inhibitors, the larvae were preincubated for 45–60 min before tail fin amputation with the respective drugs: Conoidin A (Con A, 5 μM; Cayman Chemical, Ann Arbor, MI), auranofin (Aur, 500 nM, 1 μM, 5 μM; TOCRIS Bioscience, Avonmouth, Bristol, United Kingdom), or phloretin (100 μM; Sigma-Aldrich). Drugs were present in the mounting agarose and immersion medium. Note that the effective drug bathing concentrations for zebrafish larvae are typically higher than those used in cell culture or pure enzyme experiments for various reasons, including different pharmacokinetics, target affinity, epidermal permeability, and others. Working concentrations at ~1–100 μM, as used here, are common (17). At least a 10× agarose volume equivalent of iso-E3 (~750 μL) containing inhibitors and/or H_2O_2 was added on top of the agarose pad when the acquisition started. To measure endogenous H_2O_2 gradients, larvae were wounded and mounted in regular, hypo-E3-, or iso-E3-based 1% low-melting agarose, without the addition of exogenous H_2O_2. HyPer fluorescence was excited every minute using a LED light source (Lumencor, Beaverton, OR) with 438/57 and 475/28 bandpass filters (also Lumencor). Emission was acquired using a 535/30 emission filter (Chroma Technology, Bellows Falls, VT). Images were acquired at room temperature (~26°C) using the NIS-Elements software (Nikon, Shinagawa, Tokyo) on an Eclipse Ti inverted microscope, equipped with a 20× Plan Apochromat NA 0.75 air objective lens (Nikon), an Andor Clara charge-coupled device camera (Andor Technology, Belfast, Northern Ireland) and a motorized stage.

Image processing and data analysis

All image processing was performed with the softwares FIJI (18), MATLAB R2015a (The MathWorks, Natick, MA), or the Anaconda distribution of Python, using custom scripts based on the Pandas, SciPy, NumPy, and scikit-image libraries. Background correction was performed by globally subtracting the average intensity of a region outside the larvae from the raw images. After median-filtering, the 475/28 nm excitation channel image was used to generate a mask by applying the automatic Yen threshold method (19) implemented in ImageJ/FIJI (National Institutes of Health, Bethesda, MD). To quantify HyPer signal intensity, background-subtracted and thresholded excitation ratio images were calculated, and the region outside the tail fin (namely, the notochord) was manually masked out with FIJI. Using a custom Python script, the ratio value of every pixel was remapped, that is, expressed as a function of binned distance from the wound margin. Performed on every image of the time-lapse movie, this calculation yielded a *x-y-t* matrix that was used for the following MATLAB analysis. Please see Supporting Material for analysis scripts (Data S1). Briefly, for each timepoint, background-drift was approximated using a line fit through the HyPer ratios distal to the wound margin and subtracted from the gradient profile to yield the baseline-corrected HyPer ratio (Fig. S1). Individual experiments were excluded from further analysis when H_2O_2 tissue perfusion was unusually delayed, or when the baseline correction led to distorted (for example, partly cropped/incomplete) data maps. Equivalent, baseline-corrected HyPer matrices from different experiments (for example, using the same bathing conditions, H_2O_2 concentrations) were concatenated into a single, pooled data matrix for further analysis. To calibrate HyPer, peak HyPer ratios close to the wound margin (0–100 μm) were averaged and assumed to roughly reflect H_2O_2 bath concentration. The data were interpolated with the hyperbolic function $y(x) = (x \times a)/(b + x)$, where y is the baseline-corrected HyPer ratio, x is the H_2O_2 bath concentration, and a and b are free fitting parameters. The purpose of this fitting is to generate a simple, empirical description of the HyPer dose-response in live fish. H_2O_2 concentration maps were generated by applying the inverse dose-response function (that is, $x(y)$) on each field of the baseline-corrected HyPer matrices. For kinetic analysis, only nonsaturated HyPer ratios corresponding to $[H_2O_2] < 15$ μM were used, and 10 μM H_2O_2 experiments were excluded from kinetic analysis due to high noise and low sample size. Calibrated H_2O_2 matrices were smoothed and subjected to pixel-by-pixel analysis of spatial and temporal changes in local $[H_2O_2]$. For smoothing along the space dimension, we used the third-party MATLAB "smooth2a" function (by Greg Reeves, Caltech, Pasadena, CA). In our script, smooth2a replaces each H_2O_2 concentration field $P_x(t)$ of the unsmoothed H_2O_2 concentration matrix by the mean of $P_x(t)$ and its three neighboring concentration fields to the left and right (that is, from $P_{x-3}(t)$ to $P_{x+3}(t)$). From the smoothed concentration matrices, tissue reaction rates ($f(P)$) were calculated per Eq. 3 (see Results). The substrate inhibition function $f(P)_{fit} = V_{max} \times P/(K_m + P + P^2/K_i)$ was fitted to these data to derive kinetic parameters (20). Fitting was performed using the MATLAB "fit" function (nonlinear least square and least absolute residual method, see script). This function assumes reversibility of inhibition. For substrate inhibition through overoxidation of peroxiredoxin to sulfinic acid (14), reversibility is plausible to assume (21). Yet not all higher oxidation states of cysteine are readily reversible, so this equation is an approximation. We also evaluated the dependence of H_2O_2 reaction rate on a H_2O_2 diffusion constant by repeating the calculations for $D = 500$ $\mu m^2/s$ and $D = 2000$ $\mu m^2/s$ (extreme values of plausible H_2O_2 diffusivity; Fig. S2 *a*). To test the robustness of our Laplacian approximation method, we also used a five-point-stencil instead of the standard three-point-stencil (Data S1), with little effect on the result (Fig. S2 *b*).

RESULTS

Imaging H_2O_2 reaction-diffusion with HyPer in live zebrafish larvae

To probe H_2O_2 reaction-diffusion in live tissues, we perfused zebrafish larvae expressing the genetically encoded H_2O_2 sensor HyPer (7,22) with defined bath concentrations of H_2O_2 (Fig. 1 *A*). HyPer is expressed in the cytoplasm, so tissue H_2O_2 gradients are measured by the fraction of extracellular H_2O_2 that enters cells. The high H_2O_2 reactivity of OxyR ($k \sim 10^5$ M^{-1} s^{-1}) (23), albeit lower than that of peroxiredoxin ($k \sim 10^7$ M^{-1} s^{-1}) (12), allows the HyPer sensor to detect cytoplasmic H_2O_2 with reasonable sensitivity.

Intact zebrafish epidermis is little permeable to H_2O_2, but H_2O_2 can enter fish through an epithelial breach generated

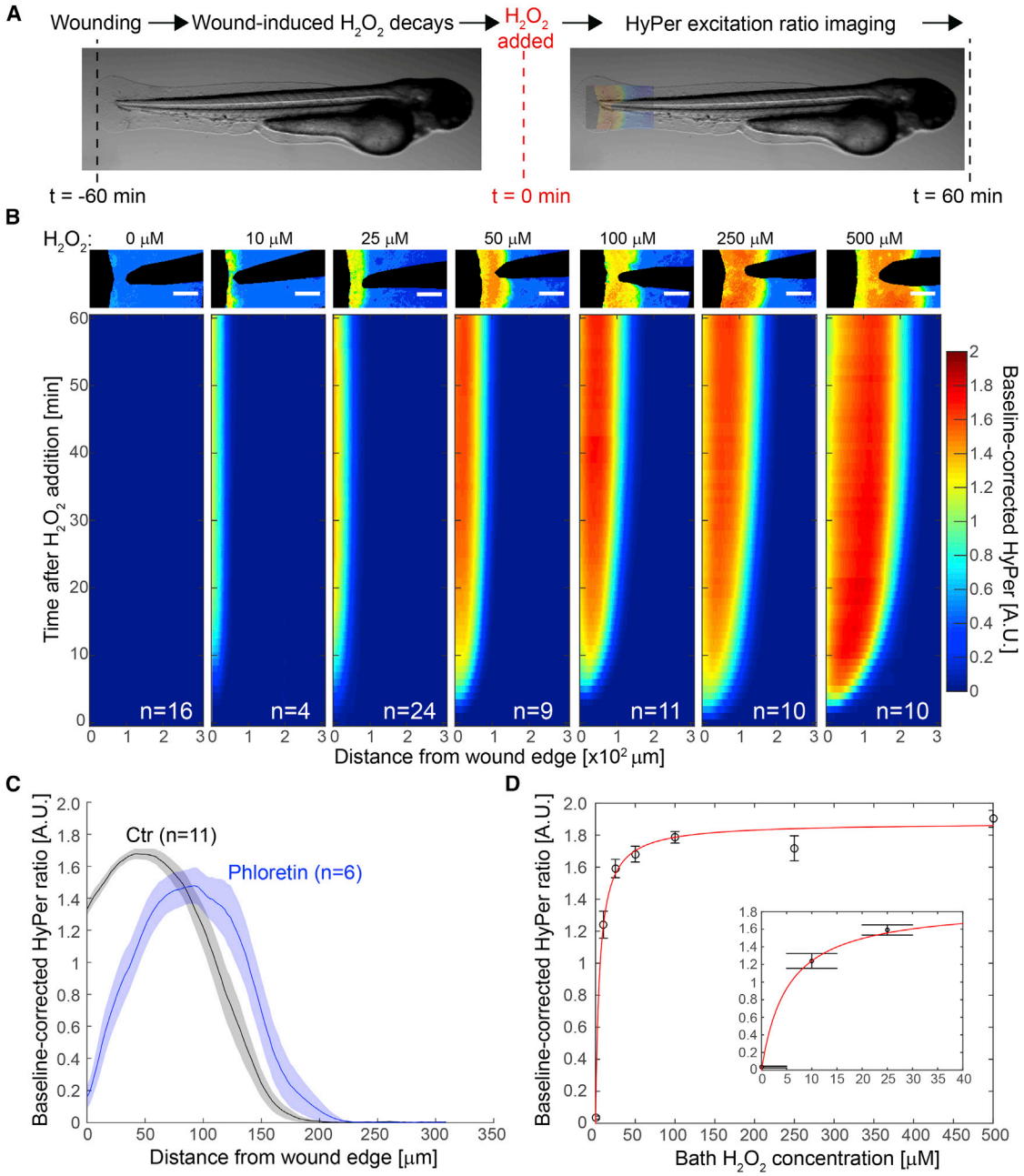

FIGURE 1 Imaging H_2O_2 reaction-diffusion in live zebrafish larvae. (*A*) Experimental scheme is given. Tail fin-amputated zebrafish larvae are perfused with defined concentrations of H_2O_2 after the endogenous, wound-induced H_2O_2 gradient has subsided. Tissue H_2O_2 is imaged with the genetically encoded biosensor HyPer. (*B*) HyPer ratio-imaging of tissue H_2O_2 after perfusion with indicated concentrations of bath H_2O_2 is given. (*Top panels*) Representative, color-coded HyPer ratio images $t = 60$ min after H_2O_2 addition are shown. (*Lower panels*) Spatiotemporal plots of baseline-corrected and color-coded HyPer ratio versus time after H_2O_2 addition and distance from wound edge are shown; *N*, number of animals in experiment. Scale bars represent 100 μm. (*C*) Average profile plots of exogenous H_2O_2 gradient with/without aquaporin inhibition (100 μM phloretin) at 60 min after H_2O_2 addition are given. Ctr, 100 μM H_2O_2 control (data from Fig. 1 *B*) is shown. Phloretin, 100 μM H_2O_2 and phloretin treatment is shown. (*Shaded area*) Mean ± SEM. (*D*) HyPer calibration curve is given. Bath H_2O_2 concentration is plotted against the HyPer signal near the wound margin, where it is assumed to roughly reflect bath $[H_2O_2]$. Data from Fig. 1 *B* is used. (*Fitted line*) Dose-response curve is given. (*Inset*) Focusing in on the initial part of the data used for later calculation of reaction rates (5 μM > $[H_2O_2]$ > 0.2 μM), as shown. Error bars, Mean ± SEM of number of animal experiments detailed in Fig. 1 *B*. To see this figure in color, go online.

by tail fin tip amputation (24). To warrant persistent perfusion of the tissue with bath H_2O_2, we blocked closure of the amputation wound by immersing the fish in isotonic solution during the entire experiment (24). Tail fin wounding triggers endogenous, extracellular H_2O_2 synthesis through the epithelial NADPH oxidase Duox as previously described in Niethammer et al. (7). After dissipation of the endogenous H_2O_2 signal (~60 min after injury), we added

10–500 μM H_2O_2 to the isotonic fish bathing solution and followed H_2O_2 diffusion by fluorescence imaging of HyPer (Fig. 1 *A*).

Diffusion of bath H_2O_2 into the tail fin gave rise to exogenous, tissue-scale HyPer gradients (Fig. 1 *B*; Movies S1, S2, S3, S4, S5, and S6). HyPer levels reached their maximum >25 μM bath H_2O_2 indicating saturation of the biosensor. If H_2O_2 diffusion were the only factor determining spatial propagation of extracellular H_2O_2 signals into the tissue, as sometimes assumed for simplification (25), HyPer gradients should continuously expand into the animal. By contrast, the spatial gradients stabilized >40 min at distinct penetration depths depending on bath H_2O_2 concentration (Fig. 1 *B*). The steady states suggest that H_2O_2 diffusion is counterbalanced by H_2O_2 degradation in the tissue. Most H_2O_2 breakdown occurs inside cells where most antioxidants reside. Accordingly, limiting H_2O_2 access to the cell cytoplasm with the aquaporin inhibitor phloretin (26) increased H_2O_2 penetration depth into the tissue (Fig. 1 *C*). As expected, the effects of phloretin inhibition were highest close to the wound margin (<80 μm), where the tissue concentration of phloretin was likely highest. Likewise, high bath $[H_2O_2]$ (that is, >250 μM) decreased HyPer signals near the wound, in line with previous results showing that high $[H_2O_2]$ inhibits H_2O_2 uptake into yeast cells (27). Close to the wound margin, we assume that bath $[H_2O_2]$ is little altered by degradation (that is, $[H_2O_2]_{\text{tissue}} \approx [H_2O_2]_{\text{bath}}$). To generate a HyPer calibration curve, we plotted baseline-corrected HyPer peak-ratios close to the wound margin versus bath $[H_2O_2]$. This plot was fitted with a dose-response curve to convert HyPer signals into H_2O_2 concentrations (Fig. 1 *D*).

Inferred reaction rates reveal substrate inhibition of H_2O_2 degradation in vivo

Owing to the flatness of the larval zebrafish tail fin, H_2O_2 diffusion through this tissue can be conceptualized as a one-dimensional reaction-diffusion problem, where the point source of H_2O_2 is the wound margin (that is, where bath H_2O_2 enters the tissue). Assuming Fickian diffusion, the following equation describes local H_2O_2 concentration changes ($\partial P/\partial t$) as a function of H_2O_2 diffusion ($D(\partial^2 P/\partial x^2)$) and reaction ($f(P)$):

$$\frac{\partial P}{\partial t} = D\frac{\partial^2 P}{\partial x^2} + f(P). \quad (1)$$

P is the local H_2O_2 concentration, t is time, D is the H_2O_2 diffusivity through the tissue, x is the distance to the wound, and $f(P)$ is the local net reaction rate. We converted this continuous reaction-diffusion equation into a discrete equation, as follows:

$$\frac{\Delta P}{\Delta t} \approx D\frac{\Delta^2 P}{\Delta x^2} + f(P). \quad (2)$$

The discretization steps are the spatiotemporal resolution values of our data, that is, $\Delta x = 2.6$ μm and $\Delta t = 1$ min (Fig. 2 *A*). The diffusion term in this equation (first term on the right-hand side) is the discrete Laplace operator; it is a function of the local concentration P and the concentration in its nearest neighbors: P_{x^+} and P_{x^-}. The change term (left-hand side of Eq. 2) is the difference between the local H_2O_2 at time t and its value in the same location at the previous time step: $P - P_{t^-}$. We calculated a local rate of $[H_2O_2]$ change in the following:

$$f(P) = \frac{P - P_{t^-}}{\Delta t} - \frac{D}{\Delta x^2}(P_{x^+} + P_{x^-} - 2P). \quad (3)$$

Here, we used $D = 1000$ $\mu m^2/s$ (28). For calculating P, baseline-corrected HyPer signals were converted to H_2O_2 concentrations by applying the calibration function determined above (see Fig. 1 *D*). Near the saturated region of HyPer (>1.4), reaction rates became increasingly noisy, so we excluded the near-saturated HyPer regime. We calculated $f(P)$ from the 25 to 500 μM H_2O_2 reaction-diffusion data (Fig. 1 *B*) using Eq. 3, and plotted the result as function of P (Fig. 2 *B*). Despite the differences in gradient appearance and penetration depth, all data collapsed onto the same kinetic relationship, regardless of bath H_2O_2 concentration. For $[H_2O_2]$ <2 μM, H_2O_2 degradation increased with $[H_2O_2]$, then leveled off and decreased close to zero at ~8–10 μM. We combined the data from all 64 animal experiments into one graph (Fig. 2 *C*). A simple substrate inhibition model fitted the data well, corroborating the idea that H_2O_2 inhibits its own degradation at higher concentrations. Overoxidation of peroxiredoxin, one of the major H_2O_2 detoxifying enzymes in cells, may underlie this inhibition of H_2O_2 degradation as previously proposed (14). The rate constants derived by our approach ($V_{max} \sim 40$ μM/s, $K_m \sim 4$ μM; Fig. S2) are within the order of magnitude of those estimated for H_2O_2 degradation in plants, underlining their quantitative plausibility (28).

The peroxiredoxin-thioredoxin antioxidant chain limits H_2O_2 reaction-diffusion in tissues

To test the mechanistic basis of H_2O_2 tissue degradation, we probed known antioxidant reactions (Fig. 3 *A*). We used conoidin A (Con A) to covalently inactivate peroxiredoxins (Prx), which are highly abundant and reactive, cytoplasmic H_2O_2 scavengers (29). We also inhibited regeneration of reduced thioredoxin (Trx) by blocking thioredoxin reductase with auranofin (Aur) (30). Both treatments led to significantly increased H_2O_2 penetration consistent with inhibition of H_2O_2 degradation (Fig. 3 *B*). We also noticed a counterintuitive decrease of HyPer-amplitudes in conoidin A-treated

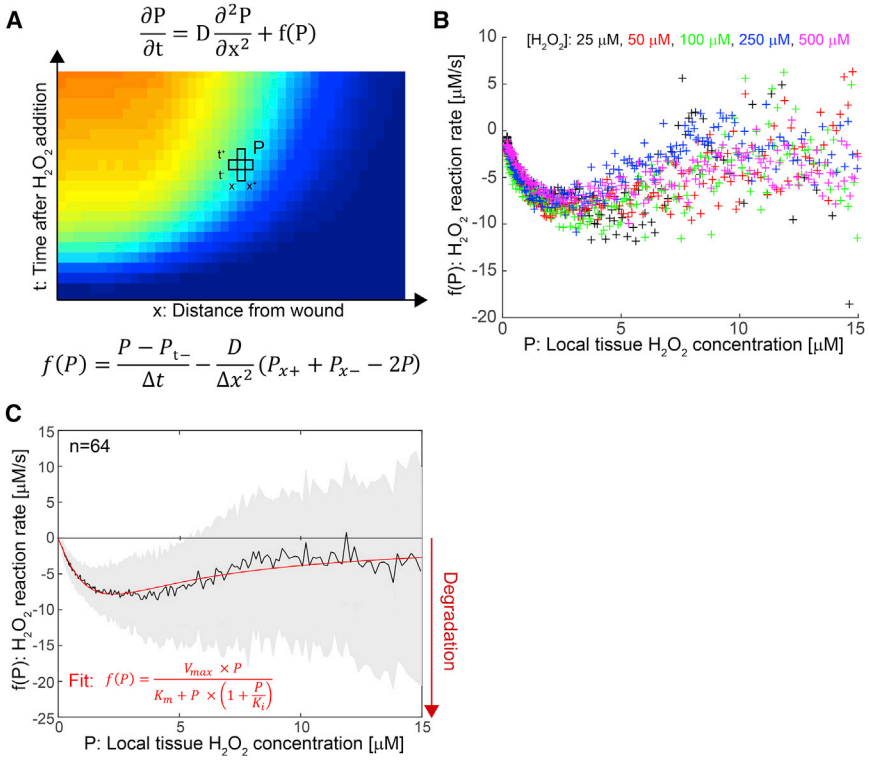

FIGURE 2 Calculation of H_2O_2 tissue reaction rates from time-lapse imaging data. (*A*) Calculation scheme is given. The equation, which describes the continuous change of local H_2O_2 concentration as a function of diffusion (first term) and reaction (second term) along one spatial dimension, was discretized and solved for tissue reaction rate $f(P)$. Δt in the respective difference equation corresponds to the time resolution of time-lapse acquisition (1 min), and Δx corresponds to the pixel size (~2.6 μm). (*B*) $f(P)$ is calculated as described above, as a function of indicated bath concentrations of H_2O_2 (*color-coded*). Plotted here is the median of the binned data without upper/lower quartiles for better clarity. (*C*) Pooled data from 25 to 500 μM H_2O_2 experiments is given. Plotted here is the median of the binned data with upper/lower quartiles. (*Fitted line/equation*) Substrate inhibition model is shown. Fit results: K_i = 1.187 μM, K_m = 4.338 μM, V_{max} = −37.78 μM/s, R^2 = 0.9997. To see this figure in color, go online.

animals (Fig. 3 *B*, *middle panel*). The reasons for this attenuation are unclear. Conoidin A amplifies the endogenous H_2O_2 gradient during the drug preincubation period (Fig. 3 *D*), which may suppress entry of external H_2O_2 in the following perfusion experiment per H_2O_2-induced H_2O_2 uptake inhibition (27). H_2O_2 reaction rates calculated from auranofin-treated animals became too noisy >5 μM H_2O_2. For low [H_2O_2], they revealed a dose-dependent inhibition of H_2O_2 degradation compared to untreated controls (Fig. 3 *C*), corroborating the quantitative validity of our kinetic inference method.

Wound-induced H_2O_2 gradients break antioxidant barriers close to the wound margin

Endogenous H_2O_2 gradients were regulated like the ectopic patterns: Conoidin A strongly enhanced HyPer signals within ~100 μm of the wound margin, regardless of whether larvae were wounded under normal freshwater conditions, or conditions where wound closure was inhibited by isotonic bathing solution. The stimulating effect of conoidin A on wound-induced HyPer signals (Fig. 3 *D*) contrasts its counterintuitive, suppressive effect on H_2O_2-bathing-induced HyPer signals (Fig. 3 *B*). The latter but not the former experiment involves preincubation of larvae with conoidin A. The drug augments accumulation of wound-derived H_2O_2 during the preincubation period. This may suppress H_2O_2 uptake in the subsequent bathing experiment, quenching HyPer responses to exogenous H_2O_2 as discussed above. Oddly, auranofin increased wound-induced HyPer signals only after isotonic injury, but had little effect on hypotonic wounds (Fig. S3). Isotonic wounds close slowly, which allows persistent tissue perfusion with compounds that otherwise poorly permeate the intact zebrafish epidermis (for example, H_2O_2). By contrast, hypotonic wounds close fast (24), providing only a short time window for perfusion. Insufficient drug perfusion is the simplest explanation for why auranofin is little effective on hypotonic wounds.

We calibrated wound-induced HyPer gradients using the dose-response function in Fig. 1 *D*. On average, endogenous H_2O_2 gradients do not exceed peak concentrations of 5 μM extracellular H_2O_2. As shown above, antioxidant reactions become exhausted above 2 μM H_2O_2, when H_2O_2 degradation rate stops to increase with increasing [H_2O_2] (Fig. 2 *C*). In the endogenous, wound-induced H_2O_2 gradients such high concentrations occur within ~30 μm of the wound margin (Fig. 4).

DISCUSSION

Paracrine signaling functions of extracellular H_2O_2 are intriguing, but quantitative aspects of H_2O_2 tissue signaling need to be better defined. We demonstrate the physiological significance of aquaporin-mediated cellular uptake, and Prx-Trx-mediated cytoplasmic breakdown of H_2O_2 for tissue-scale redox pattern formation. Our analysis provides a quantitative baseline for comparing the signaling kinetics of H_2O_2 to that of other early wound signals (25). It

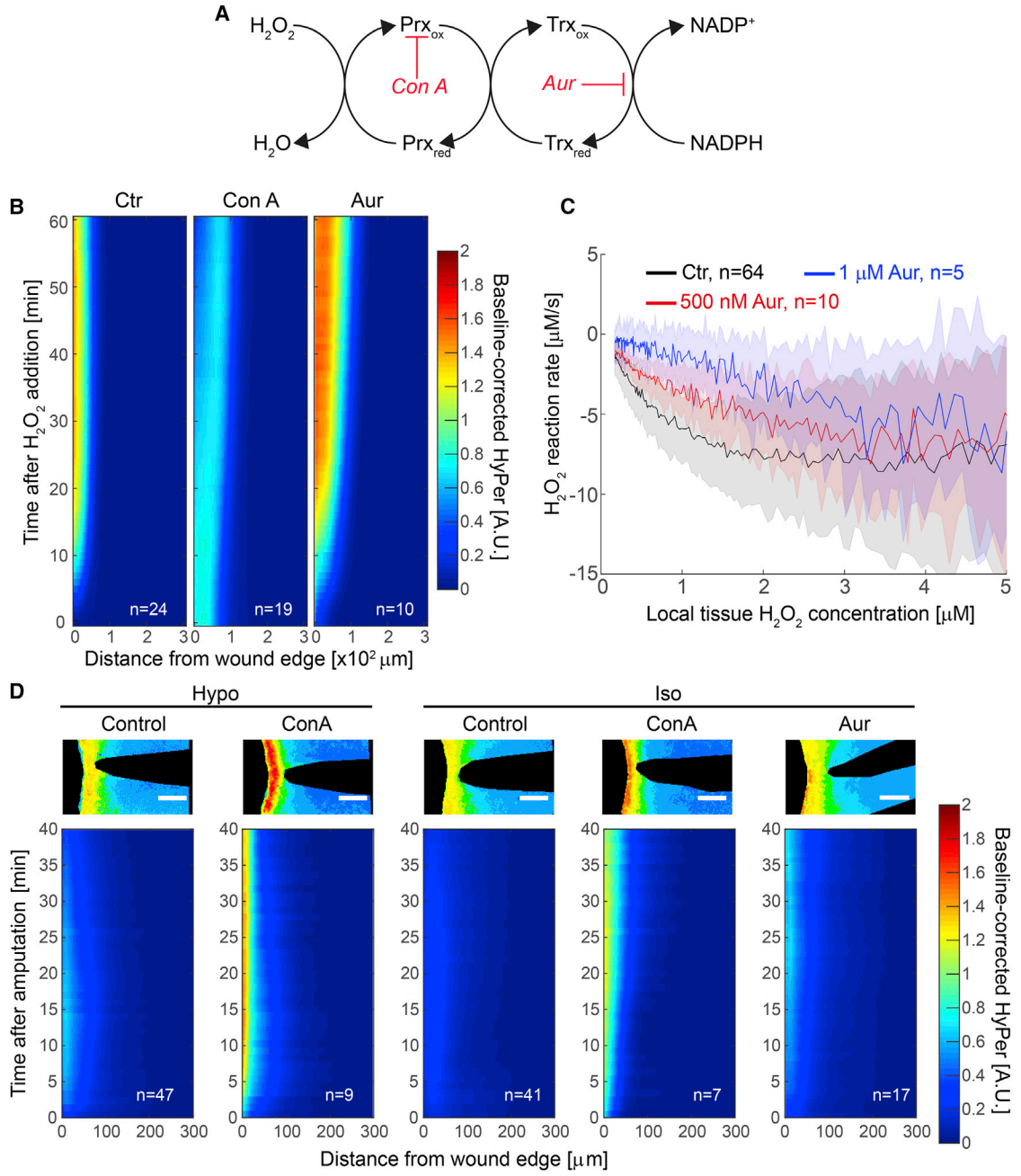

FIGURE 3 The Prx-Trx antioxidant chain limits H_2O_2 reaction-diffusion in tissues. (*A*) Scheme of Prx-Trx antioxidant chain with pharmacologic inhibitors is given. (*B*) Spatiotemporal plots of baseline-corrected and color-coded HyPer ratio at 25 μM bath H_2O_2 in the absence (Ctr) or presence of 5 μM Con A to inhibit peroxiredoxin, and 500 nM Aur to inhibit thioredoxin reductase, are shown. The control dataset corresponds to the 25 μM dataset in Fig. 1 *B*. (*C*) Plots of $f(P)$ at 500 nM and 1 μM Aur are given. Plotted here is the median of the binned data with upper/lower quartiles. (*D*) Wound-induced H_2O_2 gradients (that is, no exogenous H_2O_2 added) are given. (*Top panels*) Representative, color-coded HyPer ratio images $t = 25$ min after injury are shown. (*Lower panels*) Baseline-corrected and color-coded spatiotemporal plots of wound-induced H_2O_2 gradient formation in the absence or presence of antioxidant chain inhibitors (5 μM Con A, 5 μM Aur) are shown. (*Hypo*, wounding performed in normal, hypoosmotic fish bathing solution; *Iso*, wounding performed in isosmotic fish bathing solution; *N*, number of animal experiments). To see this figure in color, go online.

indicates self-inhibition of H_2O_2 breakdown, although the mechanism of substrate inhibition remains to be identified. Overoxidation of peroxiredoxin (14) or NADPH depletion may be conceived.

Our data suggest that antioxidant barriers are not overwhelmed farther than 30 μm away from the wound margin. Per the consensus model of redox signaling through redox-sensitive cysteine switches, this means that the wound-induced H_2O_2 gradient unlikely modulates redox signaling in distant leukocytes, unless the respective redox sensor in/on leukocytes is as H_2O_2-reactive as HyPer or peroxiredoxin ($k \sim 10^5$–10^7 M^{-1} s^{-1}), or antioxidant competition

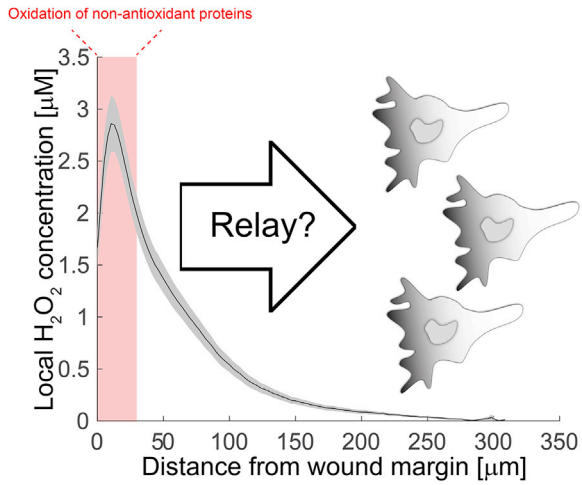

FIGURE 4 Redox signaling by the endogenous, wound-induced H_2O_2 gradient may occur close to the wound margin. Average profile plot of the wound-induced, endogenous H_2O_2 gradient (from data in Fig. 3 *D*) at 20 min after injury is given. (*Gray shaded curve area*) Mean ± SEM. (*Shaded rectangle*) Region where antioxidant floodgates are likely to be broken ($[H_2O_2]>2$ μM) is shown. Cartoon representation of leukocytes at distances from which they initially respond to wounds. To see this figure in color, go online.

is annulled in some hypothetical, subcellular reactive oxygen species microenvironment (31) invisible to our imaging assay. It will be interesting to determine the H_2O_2 reactivity of Lyn, and other SRC kinases, as those were shown to act as redox sensors during the wound response (1,10).

Are there alternative models that explain Duox-mediated leukocyte chemotaxis to wounds (32)? Our data cannot exclude that a H_2O_2 receptor exists in/on leukocytes that senses H_2O_2 akin to how guanylyl cyclase detects nitric oxide (33). Likewise, redox relay signaling through oxidized intermediates of the antioxidant chain remains a possibility (34). By consuming NADPH, NADPH oxidases, such as Duox, directly alter the NADPH/$NADP^+$ ratio upon extracellular signals. Enzymes whose activity depends on this ratio, such as $NADP^+$-dehydrogenases, could serve as a sensor mechanism. Concordantly, we recently identified an oxidized arachidonate metabolite generated by $NADP^+$-dehydrogenase activity as an early wound chemoattractant in zebrafish (15,35).

CONCLUSION

We have developed an image-based method to quantify H_2O_2 reaction-diffusion reaction kinetics in live animals. Our data suggest that direct redox signaling by wound-derived H_2O_2 is highly confined to the wound margin.

SUPPORTING MATERIAL

Three figures, one data file, and six movies are available at http://www.biophysj.org/biophysj/supplemental/S0006-3495(17)30340-5.

AUTHOR CONTRIBUTIONS

P.N. conceived the study. P.N. did the MATLAB analysis and prepared the figures. P.N. and J.B.X. wrote the manuscript. J.B.X. conceived the reaction-diffusion analysis method, and supervised its implementation by P.N. B.E. coded the Python scripts for image processing. M.J., P.N., and B.E conducted the experiments. M.J. and B.E. processed the imaging data. All authors read, commented on, and agreed to the final version of the manuscript.

ACKNOWLEDGMENTS

Research was supported by the National Institutes of Health grant No. GM099970, an American Asthma Foundation Scholar Grant to P.N., the Memorial Sloan Kettering Cancer Center Functional Genomics Initiative, and in part through the National Institutes of Health/National Cancer Institute Cancer Center Support Grant No. P30CA008748.

REFERENCES

1. Yoo, S. K., C. M. Freisinger, …, A. Huttenlocher. 2012. Early redox, Src family kinase, and calcium signaling integrate wound responses and tissue regeneration in zebrafish. *J. Cell Biol.* 199:225–234.
2. Love, N. R., Y. Chen, …, E. Amaya. 2013. Amputation-induced reactive oxygen species are required for successful *Xenopus* tadpole tail regeneration. *Nat. Cell Biol.* 15:222–228.
3. Moreira, S., B. Stramer, …, P. Martin. 2010. Prioritization of competing damage and developmental signals by migrating macrophages in the *Drosophila* embryo. *Curr. Biol.* 20:464–470.
4. Razzell, W., I. R. Evans, …, W. Wood. 2013. Calcium flashes orchestrate the wound inflammatory response through DUOX activation and hydrogen peroxide release. *Curr. Biol.* 23:424–429.
5. Gauron, C., F. Meda, …, S. Vriz. 2016. Hydrogen peroxide (H_2O_2) controls axon pathfinding during zebrafish development. *Dev. Biol.* 414:133–141.
6. Gauron, C., C. Rampon, …, S. Vriz. 2013. Sustained production of ROS triggers compensatory proliferation and is required for regeneration to proceed. *Sci. Rep.* 3:2084.
7. Niethammer, P., C. Grabher, …, T. J. Mitchison. 2009. A tissue-scale gradient of hydrogen peroxide mediates rapid wound detection in zebrafish. *Nature.* 459:996–999.
8. Enyedi, B., and P. Niethammer. 2015. Mechanisms of epithelial wound detection. *Trends Cell Biol.* 25:398–407.
9. Finkel, T. 2011. Signal transduction by reactive oxygen species. *J. Cell Biol.* 194:7–15.
10. Yoo, S. K., T. W. Starnes, …, A. Huttenlocher. 2011. Lyn is a redox sensor that mediates leukocyte wound attraction in vivo. *Nature.* 480:109–112.
11. Evans, I. R., F. S. L. M. Rodrigues, …, W. Wood. 2015. Draper/CED-1 mediates an ancient damage response to control inflammatory blood cell migration in vivo. *Curr. Biol.* 25:1606–1612.
12. Winterbourn, C. C. 2013. The biological chemistry of hydrogen peroxide. *Methods Enzymol.* 528:3–25.
13. Rhee, S. G., S. W. Kang, …, K. Kim. 2001. Peroxiredoxin, a novel family of peroxidases. *IUBMB Life.* 52:35–41.
14. Wood, Z. A., L. B. Poole, and P. A. Karplus. 2003. Peroxiredoxin evolution and the regulation of hydrogen peroxide signaling. *Science.* 300:650–653.
15. Enyedi, B., S. Kala, …, P. Niethammer. 2013. Tissue damage detection by osmotic surveillance. *Nat. Cell Biol.* 15:1123–1130.
16. Nüsslein-Volhard, C., and R. Dahm. 2002. Zebrafish: A Practical Approach. Oxford University Press, New York.

17. Wittmann, C., M. Reischl, …, C. Grabher. 2015. A zebrafish drug-repurposing screen reveals sGC-dependent and sGC-independent pro-inflammatory activities of nitric oxide. *PLoS One.* 10:e0137286.

18. Schindelin, J., I. Arganda-Carreras, …, A. Cardona. 2012. FIJI: an open-source platform for biological-image analysis. *Nat. Methods.* 9:676–682.

19. Yen, J. C., F. J. Chang, and S. Chang. 1995. A new criterion for automatic multilevel thresholding. *IEEE Trans. Image Process.* 4:370–378.

20. Copeland, R. M. 2000. Enzymes. Wiley, New York.

21. Woo, H. A., H. Z. Chae, …, S. G. Rhee. 2003. Reversing the inactivation of peroxiredoxins caused by cysteine sulfinic acid formation. *Science.* 300:653–656.

22. Belousov, V. V., A. F. Fradkov, …, S. Lukyanov. 2006. Genetically encoded fluorescent indicator for intracellular hydrogen peroxide. *Nat. Methods.* 3:281–286.

23. Kóna, J., and T. Brinck. 2006. A combined molecular dynamics simulation and quantum chemical study on the mechanism for activation of the OxyR transcription factor by hydrogen peroxide. *Org. Biomol. Chem.* 4:3468–3478.

24. Gault, W. J., B. Enyedi, and P. Niethammer. 2014. Osmotic surveillance mediates rapid wound closure through nucleotide release. *J. Cell Biol.* 207:767–782.

25. Weavers, H., J. Liepe, …, M. P. H. Stumpf. 2016. Systems analysis of the dynamic inflammatory response to tissue damage reveals spatiotemporal properties of the wound attractant gradient. *Curr. Biol.* 26:1975–1989.

26. Fischbarg, J., L. S. Liebovitch, and J. P. Koniarek. 1987. Inhibition of transepithelial osmotic water flow by blockers of the glucose transporter. *Biochim. Biophys. Acta.* 898:266–274.

27. Folmer, V., N. Pedroso, …, H. S. Marinho. 2008. H_2O_2 induces rapid biophysical and permeability changes in the plasma membrane of *Saccharomyces cerevisiae*. *Biochim. Biophys. Acta.* 1778:1141–1147.

28. Vestergaard, C. L., H. Flyvbjerg, and I. M. Møller. 2012. Intracellular signaling by diffusion: can waves of hydrogen peroxide transmit intracellular information in plant cells? *Front. Plant Sci.* 3:295.

29. Haraldsen, J. D., G. Liu, …, G. E. Ward. 2009. Identification of conoidin A as a covalent inhibitor of peroxiredoxin II. *Org. Biomol. Chem.* 7:3040–3048.

30. Gromer, S., L. D. Arscott, …, K. Becker. 1998. Human placenta thioredoxin reductase. Isolation of the selenoenzyme, steady state kinetics, and inhibition by therapeutic gold compounds. *J. Biol. Chem.* 273:20096–20101.

31. Woo, H. A., S. H. Yim, …, S. G. Rhee. 2010. Inactivation of peroxiredoxin I by phosphorylation allows localized H_2O_2 accumulation for cell signaling. *Cell.* 140:517–528.

32. Enyedi, B., and P. Niethammer. 2013. H_2O_2: a chemoattractant? *Methods Enzymol.* 528:237–255.

33. Russwurm, M., and D. Koesling. 2004. NO activation of guanylyl cyclase. *EMBO J.* 23:4443–4450.

34. Sobotta, M. C., W. Liou, …, T. P. Dick. 2015. Peroxiredoxin-2 and STAT3 form a redox relay for H_2O_2 signaling. *Nat. Chem. Biol.* 11:64–70.

35. Erlemann, K.-R., C. Cossette, …, W. S. Powell. 2007. Regulation of 5-hydroxyeicosanoid dehydrogenase activity in monocytic cells. *Biochem. J.* 403:157–165.